Signal Interception: Performance Advantages of Cyclic-Feature Detectors

William A. Gardner, *Fellow, IEEE,* and Chad M. Spooner, *Student Member, IEEE,*

Abstract— **The problem of detecting the presence of spread-spectrum phase-shift-keyed signals in variable noise and interference backgrounds is considered, and the performances of four detectors are evaluated and compared. These include the optimum radiometer, the optimum modified radiometer that jointly estimates the noise level and detects the signal, and the maximum-SNR spectral-line regenerator for spectral line frequencies equal to the chip rate and the doubled carrier frequency. It is concluded that the spectral line regenerators can outperform both types of radiometers by a wide margin. The performance advantages are quantified in terms of receiver operating characteristics for several noise and interference environments and receiver collection times.**

I. Introduction

ATTEMPTED interception of communication signals that arise from modulation schemes designed to foil such interception is a topic that is receiving increasing attention. In light of the growing use of direct-sequence spread-spectrum techniques and the increasingly congested communication environments, standard methods of interception, which are based on energy measurement, and are collectively referred to as *radiometry,* are becoming less effective. In particular, since radiometric methods simply measure energy in specific bands of frequencies, they are inherently susceptible to unknown or changing background noise level and interference activity. In order to design secure communication systems, it is necessary to assess the vulnerability of competing techniques to interception. For this purpose, the approach of designing and analyzing the performance of detectors that are capable of intercepting spread-spectrum signals in adverse environments where radiometric methods are likely to fail is taken in this paper.

Communication signals have traditionally been modeled as stationary random processes. Although communication signals typically involve one or more periodicities underlying their random fluctuations, due to sine-wave carriers and repetitive pulsing or keying, a stationary model can be obtained by introducing random phase variables uniformly distributed over one period of each periodicity [1]. On the surface this seems appropriate if the receiver has no knowledge of carrier phase or clock timing and is, therefore, unsynchronized to the periodicities. However, by looking beneath the surface we find that carrier and clock periodicity can indeed be exploited by receivers that have no knowledge of the associated phases, and that make no attempt to estimate those phases. This has been demonstrated in [2] where it is explained that, in comparison with the optimum quadratic detector for the stationary model of the signal, superior detection performance (i.e., detection of the presence of a weak signal in noise) can be obtained by exploiting the single frequency of some harmonic of a periodicity, such as a doubled carrier frequency, or a keying rate. It has also been demonstrated in [3] where, in comparison with a conventional estimator (based on a stationary model of the signal) of time-difference-of-arrival (TDOA) for locating a signal source, superior estimation performance can be obtained by exploiting the doubled carrier frequency or the keying rate. No use of the phase associated with the single sine-wave frequency is made in either of these applications. This is partially analogous to the common procedure of detecting the presence of an additive sine wave in noise by measuring the magnitude of the correlation of the noisy data with a complex sine wave of arbitrary phase. But, for detection of communication signals, the problem is more subtle since such signals rarely contain additive sine-wave components (which result in spectral lines).

In the signal detection techniques studied in this paper, the underlying periodicities of communication signals are exploited by quadratically processing the received data. Certain simple quadratic processors are widely used to regenerate sinewaves; for instance, a squarer is often used to regenerate a sinewave with frequency equal to the doubled carrier, and a delay-and-multiply device with delay equal to half of the chip interval can be used to regenerate a spectral line at the chip rate. By using the mathematical framework of cyclostationarity, it is possible to characterize all spectral lines that can be regenerated and to solve for the quadratic transformation of the data that yields the strongest possible spectral line at a given frequency [2]. Thus, the theory of cyclostationarity provides a rigorous framework for understanding ad hoc spectral-line generators, as well as allowing for the specification of optimal spectral-line generators, which are more general than squarers and delay-and-multipliers.

The purpose of this paper is to quantify the gains in detection performance that are attainable by exploiting the underlying periodicity that is present in communication signals. More specifically, we consider phase-shift-keyed signals, which are used for spread-spectrum communications, and we determine receiver operating characteristics for operation in a relatively strong white-Gaussian-noise (WGN) background

Paper approved by the Editor for Spread Spectrum of the IEEE Communications Society. Manuscript received September 15, 1989; revised March 15, 1991. This work was supported in part by ESL, Inc., with partial matching support from the California State MICRO Program.

The authors are with the Department of Electrical Engineering and Computer Science, University of California at Davis, Davis, CA 95616.

IEEE Log Number 9105166.

0090-6778/92$03.00 © 1992 IEEE

with random fluctuations in the noise power level. In particular, we consider a nominal SNR of 0 dB, corresponding to the expected noise level, and we consider a coefficient of variation (variance normalized by squared mean) of 10% for the random fluctuation about the expected noise level. In a receiving system that monitors the noise level and adjusts the detection threshold accordingly, this 10% variation represents the error in noise-level tracking. This variation can also represent nonstationary activity of broadband interfering signals. In addition, a highly variable narrow-band interference background with SIR of -10 dB and fixed-level WGN with SNR $= 10$ dB is also considered.

The detectors whose performances are compared are the standard optimum radiometer, which is the weak-signal likelihood-ratio detector for the stationary model of the signal [4], a modified radiometer that provides the weak-signal joint maximum-likelihood estimate of the noise power level and detection of the signal (modeled as stationary), and two maximum-SNR cyclic-feature detectors (or simply cycle detectors) one of which exploits the doubled carrier frequency and the other of which exploits the keying rate.

In order to understand the operation of the cycle detectors, the signal model without the intentionally introduced random phases must be used. This model is cyclostationary rather than stationary [4]. Consequently, the concepts and definitions associated with cyclostationarity that are necessary to understand the cycle detectors are briefly reviewed in Section II. The four detectors are then defined in Section III. In order to link this study with previous studies of weak-signal detection performance [5]–[8], the detector-output SNR called deflection is evaluated in Section IV. Then in Section V, receiver operating characteristics obtained from simulations of the four detectors are presented and used to draw conclusions about performance advantages of the cycle detectors, and about the limited usefulness of deflection as a basis for comparing detectors.

II. Fundamentals of Cyclostationarity

In this section, a brief review of the basic concepts and definitions associated with cyclostationary processes is presented. A more expansive survey of both theory and applications of cyclostationarity is given in [9].

A zero-mean process $x(t)$ is said to be cyclostationary (in the wide sense) if its autocorrelation is a periodic function of time,

$$R_x(t+\tau/2, t-\tau/2) = R_x(t+T_0+\tau/2, t+T_0-\tau/2),$$

for some period $T_0 \neq 0$ where

$$R_x(t+\tau/2, t-\tau/2) \triangleq E\{x(t+\tau/2)x^*(t-\tau/2)\}, \quad (1)$$

and $E\{\cdot\}$ denotes the mathematical expectation operation. Since R_x is periodic, it admits a Fourier series representation,

$$R_x(t+\tau/2, t-\tau/2) = \sum_{\alpha} R_x^\alpha(\tau) e^{i2\pi\alpha t} \quad (2)$$

where the sum over α includes all integer multiples of the reciprocal of the fundamental period T_0. The Fourier coefficients $R_x^\alpha(\tau)$ are given by either

$$R_x^\alpha(\tau) = \frac{1}{T_0} \int_{-T_0/2}^{T_0/2} R_x(t+\tau/2, t-\tau/2) e^{-i2\pi\alpha t}\, dt, \quad (3a)$$

or

$$R_x^\alpha(\tau) = \lim_{T\to\infty} \frac{1}{T} \int_{-T/2}^{T/2} R_x(t+\tau/2, t-\tau/2) e^{-i2\pi\alpha t}\, dt. \quad (3b)$$

The function $R_x^\alpha(\tau)$, which—for each value of τ—is the strength of the sinusoid in t at frequency α in the autocorrelation $R_x(t+\tau/2, t-\tau/2)$, is referred to as the *cyclic autocorrelation.* If the process $x(t)$ is modeled as cycloergodic (which excludes all time-invariant random phases) [4], as is assumed henceforth, then the cyclic autocorrelation can be obtained from the limiting time average

$$R_x^\alpha(\tau) = \lim_{T\to\infty} \frac{1}{T} \int_{-T/2}^{T/2} x(t+\tau/2)x^*(t-\tau/2) e^{-i2\pi\alpha t}\, dt, \quad (4)$$

for any sample path of the process $x(t)$. The cycloergodic model is a natural model for the applications of interest in this paper. Clearly, the cyclic autocorrelation (3), or (4), is not identically zero for all nonzero α if and only if the autocorrelation in (3), or the lag-product of the cycloergodic process $x(t)$ in (4), contains an additive periodic component, which will be the case if $x(t)$ is cyclostationary. The set $\{\alpha\colon R_x^\alpha(\tau) \not\equiv 0\}$ is referred to as the set of *cycle frequencies.* By analogy with the terminology for the conventional autocorrelation (which is (4) with $\alpha = 0$), the Fourier transform of the cyclic autocorrelation,

$$S_x^\alpha(f) \triangleq \int_{-\infty}^{\infty} R_x^\alpha(\tau) e^{-i2\pi f\tau}\, d\tau, \quad (5)$$

is called the *cyclic spectrum.* The cyclic spectrum can also be interpreted as a spectral correlation function (SCF) according to the following characterization [9], [10]:

$$S_x^\alpha(f) = \lim_{T\to\infty} \lim_{\Delta t\to\infty} \frac{1}{T\Delta t} \cdot \int_{-\Delta t/2}^{\Delta t/2} X_T(t, f+\alpha/2) X_T^*(t, f-\alpha/2)\, dt \quad (6)$$

where

$$X_T(t,\nu) \triangleq \int_{t-T/2}^{t+T/2} x(u) e^{-i2\pi\nu u}\, du \quad (7)$$

is the complex envelope of the spectral component of $x(t)$ at frequency ν with approximate bandwidth $1/T$. Since the frequencies of the correlated spectral components are $f+\alpha/2$

and $f-\alpha/2$, the cycle frequency α is also called the *frequency separation.*

If the autocorrelation $R_x(t+\tau/2, t-\tau/2)$ or the lag product $x(t+\tau/2)x^*(t-\tau/2)$ contains multiple additive periodicities, and these periodicities are incommensurate, then the cycloergodic process is called *almost cyclostationary,* after the nomenclature of *almost periodic function* used for a function that is a sum of periodic functions with incommensurate periods. In this case, the relations (2)–(7), including (3b) but not (3a), still apply; however, the sum over the cycle frequencies α in (2) must include all harmonics of all fundamental reciprocal periods present in the autocorrelation or lag product.

If for each fundamental period, an independent random phase variable, uniformly distributed over that period, is added to the time variable t in the process model $x(t)$, then the resultant phase-randomized process $\tilde{x}(t)$ will be stationary [1],

$$R_{\tilde{x}}(t+\tau/2, t-\tau/2) = R_{\tilde{x}}(\tau), \tag{8}$$

and the stationary autocorrelation is given by

$$R_{\tilde{x}}(\tau) = R_x^0(\tau). \tag{9}$$

The corresponding power spectral density function is given by

$$S_{\tilde{x}}(f) = S_x^0(f). \tag{10}$$

Example: Binary and Quaternary Phase Shift Keying. The BPSK signal

$$s(t) = \sum_{n=-\infty}^{\infty} q(t-nT_c-t_0)\cos(2\pi f_0 t + \theta_n + \phi_0) \tag{11}$$

where T_c is the chip interval, $\{\theta_n\}$ is an independent sequence of binary variables taking on the two equiprobable values 0 and π, has SCF given by (12) below ([4], [10]) for all integers k where $Q(f)$ is the Fourier transform of the pulse $q(t)$. Similarly, the QPSK signal

$$s(t) = \sum_{n=-\infty}^{\infty} q(t-nT_c-t_0)\cos(2\pi f_0 t + \theta_n + \phi_0) \tag{13}$$

where $\{\theta_n\}$ is an independent sequence of quaternary variables taking on the four equiprobable values 0, $\pi/2$, π, $3\pi/2$, has SCF equal to that of the BPSK signal for $\alpha = k/T_c$, and is identically zero for all other $\alpha \neq 0$ [4], [10]. The magnitude of these spectral correlation functions for BPSK and QPSK are graphed in Fig. 1 as the heights of surfaces above the bifrequency (f versus α) plane. For the stationary model of the signal, the power spectral density function is given by

$$S_{\tilde{s}}(f) = S_s^0(f) = \frac{1}{4T_c}\left\{|Q(f-f_0)|^2 + |Q(f+f_0)|^2\right\}. \tag{14}$$

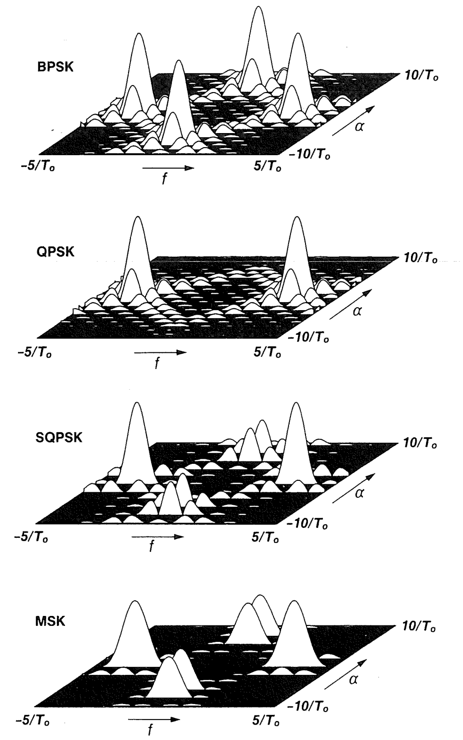

Fig. 1. Theoretical spectral correlation magnitude surfaces for BPSK, QPSK, SQPSK, and MSK modulation types.

Numerous examples of the spectral correlation function (5)–(6) for other modulated signals are given in [4], [10].

III. Radiometric and Cyclic-Feature Detectors

In this section, three basic detector structures—the radiometer, cycle detector, and joint estimation/detection radiometric (modified radiometer)—are described.

The detection problem considered here can be stated in terms of a binary hypothesis test, with the null hypothesis H_0 corresponding to signal absent ($x(t) = n(t)$) and the alternative hypothesis H_1 corresponding to signal present ($x(t) = s(t) + n(t)$) in the sliding observation interval centered at t with length T. The function $x(t)$ represents the received data, $n(t)$ is white Gaussian noise (WGN), and $s(t)$ is the zero-mean random signal of interest (SOI), which is

$$S_s^\alpha(f) = \begin{cases} \frac{1}{4T_c} Q(f+\alpha/2 \mp f_0)Q^*(f-\alpha/2 \pm f_0)e^{-i[2\pi(\alpha \mp 2f_0)t_0 \mp 2\phi_0]}, & \alpha = \pm 2f_0 + \frac{k}{T_c} \\ \frac{1}{4T_c}\{Q(f+\alpha/2+f_0)Q^*(f-\alpha/2+f_0) \\ \quad + Q(f+\alpha/2-f_0)Q^*(f-\alpha/2-f_0)\}e^{-i2\pi\alpha t_0}, & \alpha = \frac{k}{T_c}, \end{cases} \tag{12}$$

assumed to be weak and independent of the noise. Since we are concerned here with interception, the data collection parameter T of the detection devices should be large compared to the correlation time (approximate width of the autocorrelation function) of the SOI or, equivalently, the reciprocal of the bandwidth of the SOI. For example, for a spread-spectrum PSK SOI, the collect time T should greatly exceed the chip interval T_c.

For weak Gaussian signals in WGN, the maximum-likelihood (ml) signal detection criterion leads to the following approximate sufficient statistic [11]:

$$y_{\mathrm{ml}}(t) \propto \int_{t-T/2}^{t+T/2} \int_{t-T/2}^{t+T/2} R_s(u,v)x(u)x^*(v)\,du\,dv. \tag{15}$$

It can be shown that this quadratic form is asymptotically (input SNR $\to$ 0) optimal even when the weak SOI is not Gaussian [12], [13]. Thus, for weak-signal detection, the optimum detector implements a quadratic transformation of the received data and compares the resultant statistic to a threshold. Many of the ad hoc detection schemes that have been proposed for signal interception, such as the delay-and-multiply chip-rate-feature detector, the filter-squarer carrier-feature detector, and the ambiguity function, can be expressed in the general form of a quadratic transformation

$$y(t) = \int_{t-T/2}^{t+T/2} \int_{t-T/2}^{t+T/2} k(u,v)x(u)x^*(v)\,du\,dv \tag{16}$$

for some kernel $k(u,v)$ [2]. Thus, the study of the optimum detector (15) provides a benchmark for evaluation for various suboptimum and ad hoc quadratic detectors.

The actual device specified by (15) depends on the particular signal model employed. If the signal is modeled as (almost) cyclostationary, then the autocorrelation is given by (2) and the resulting device can be expressed as a *multicycle detector* [2], [10],

$$y_{mc}(t) = \sum_{\alpha} \int_{-\infty}^{\infty} S_s^{\alpha}(f)^* S_{x_T}^{\alpha}(t,f)\,df \tag{17}$$

where the sum is over all α for which the SCF $S_s^{\alpha}(f)$ is not identically zero. The function

$$S_{x_T}^{\alpha}(t,f) \triangleq \frac{1}{T} X_T(t, f+\alpha/2) X_T^*(t, f-\alpha/2) \tag{18}$$

where $X_T(t,\nu)$ is defined in (7), is called the *cyclic periodogram* (cf. [10]).

If the signal is modeled as stationary, then only the $\alpha = 0$ term in (17) is nonzero and we obtain the *optimum radiometer*

$$y_r(t) = \int_{-\infty}^{\infty} S_s^0(f) S_{x_T}^0(t,f)\,df. \tag{19}$$

Various arguments can be construed for using the magnitude of only one $\alpha \neq 0$ term[1] in (17) [2],

$$y_{sc}(t) = \int_{-\infty}^{\infty} S_s^{\alpha}(f)^* S_{x_T}^{\alpha}(t,f)\,df. \tag{20}$$

The device that compares the magnitude of the statistic (20) to a threshold is referred to as a *single-cycle detector* (or just *cycle detector*). By way of interpretation, the cycle detector output $y_{sc}(t)$ is a measure of the amount of spectral correlation present in the received waveform, whereas the radiometer output $y_r(t)$ is a measure of the amount of energy present in the received waveform.

It is shown in [10] that the detectors (17) and (20) are solutions to optimization problems that do not invoke the weak-signal assumption. Specifically, among all quadratic detectors (16), the multicycle detector (17) maximizes the performance parameter known as *deflection*

$$d \triangleq \frac{|E\{y(t)|H_1\} - E\{y(t)|H_0\}|}{\sqrt{\mathrm{Var}\{y(t)|H_0\}}}, \tag{21}$$

and the single-cycle detector (20) generates from the received signal $x(t) = s(t) + n(t)$ a spectral line at frequency α with maximum power level, subject to a constraint on the output noise spectral density level at frequency α.

The final detector of interest results from considering the noise spectral height N_0 to be unknown. This detector attempts to estimate the parameter N_0, and then uses the estimate to form a detection statistic. Since the variance of continuous-time WGN is infinite, the problem of estimating N_0 is not well posed. However, for discrete-time WGN, the variance is N_0 and the problem is, indeed, well posed. Thus, we consider a discrete-time model at this point.

Since we are operating under the weak-signal assumption, the maximum-likelihood estimate of the spectral height N_0 is approximately the same on both hypotheses and is given by

$$\hat{N}_0 = \frac{1}{M}\sum_{k=1}^{M} x_k^2 \triangleq \langle x^2 \rangle \equiv \frac{1}{M}\boldsymbol{x}^T\boldsymbol{x}, \tag{22}$$

where $\boldsymbol{x}$ is the vector of M received data samples x_k. It is shown in [12] that the log-likelihood-ratio test for a weak random signal in white Gaussian noise is approximated by

$$\ln[\Lambda(x)] = \frac{\boldsymbol{x}^T\boldsymbol{K}_s\boldsymbol{x}}{2N_0^2} - \frac{M\langle \sigma_s^2\rangle}{2N_0} \gtrless \gamma, \tag{23}$$

where $\boldsymbol{K}_s \triangleq E\{\boldsymbol{s}\boldsymbol{s}^T\}$ is the covariance matrix for the vector $\boldsymbol{s}$ of signal samples from the signal s_k, and $\langle \sigma_s^2 \rangle$ is the average power of this signal. Substituting $\hat{N}_0$ from (22) in place of N_0 in (23) and assuming a long collection time $M\big(M \gg 2\gamma N_0/\langle\sigma_s^2\rangle\big)$, we obtain the generalized maximum-likelihood detection statistic

$$y_{gml} = \frac{\boldsymbol{x}^T\boldsymbol{K}_s\boldsymbol{x}}{\langle\sigma_s^2\rangle} - \boldsymbol{x}^T\boldsymbol{x}. \tag{24}$$

[1] A primary motive is to circumvent the problem that the multicycle detector cannot be implemented unless the absolute phase of the SOI [e.g., t_0 and ϕ_0 in (11)] is known, or is estimated jointly with detection.

The statistic y_{gml} can be manipulated into the form

$$y_{gml} = \frac{M}{\langle \sigma_s^2 \rangle} \sum_{\alpha} \int_{-1/2}^{1/2} \left[\tilde{S}_s^\alpha(f)^* - \delta_\alpha \langle \sigma_s^2 \rangle \right] \tilde{S}_{x_M}^\alpha(t,f)\, df \quad (25)$$

where $\tilde{S}_s^\alpha(f)$ and $\tilde{S}_{x_M}^\alpha(t,f)$ are discrete-time counterparts of (5)–(6) and (18), respectively. Specifically,

$$\tilde{S}_s^\alpha(f) = \sum_{k=-\infty}^{\infty} \tilde{R}_s^\alpha(k) e^{-i2\pi k f} \quad (26)$$

where

$$\tilde{R}_s^\alpha(k) = \lim_{M\to\infty} \frac{1}{2M+1} \sum_{n=-M}^{M} x(n+|k|)x^*(n) \cdot e^{-i2\pi\alpha(n+|k|/2)}; \quad (27)$$

and

$$\tilde{S}_{x_M}^\alpha(t,f) = \frac{1}{M} \tilde{X}_M(t, f+\alpha/2) \tilde{X}_M^*(t, f-\alpha/2) \quad (28)$$

where

$$\tilde{X}_T(t,f) = \sum_{u=t-M}^{t-1} x(u) e^{-i2\pi f u}. \quad (29)$$

The statistic (25) differs from the discrete-time version of the multicycle detector (17) only in the $\alpha = 0$ (radiometric) term,

$$y_{mr} = \frac{M}{\langle \sigma_s^2 \rangle} \int_{-1/2}^{1/2} \left[\tilde{S}_s^0(f) - \langle \sigma_s^2 \rangle \right] \tilde{S}_{x_M}^0(t,f)\, df. \quad (30)$$

This term can be reexpressed as

$$y_{mr} = M \sum_{k=-(M-1)}^{M-1} \left[\frac{\tilde{R}_s^0(k)}{\langle \sigma_s^2 \rangle} - \delta_k \right] \tilde{R}_{x_M}^0(t,k) \quad (31)$$

where $\tilde{R}_s^0(k)$ is given by (27) with $\alpha = 0$ and

$$\tilde{R}_{x_M}^0(t,k) = \frac{1}{M} \sum_{n=t-M}^{t-|k|-1} x(n+|k|)x^*(n). \quad (32)$$

Thus, the detection statistic y_{mr}, which is called the *modified radiometer,* is simply the radiometric statistic with a reduction proportional to the noise-level estimate $(1/M)\boldsymbol{x}^T\boldsymbol{x} = \tilde{R}_{x_M}^0(t,0)$. This detector is actually the generalized maximum-likelihood detector for a weak *stationary* signal in white Gaussian noise with unknown noise level N_0. The reduction in (30) or in (31) can be extreme for wideband signals, where $\tilde{R}_s^0(k)/\langle \sigma_s^2 \rangle \cong \delta_k$ in (31) or where $\tilde{S}_s^0(f)/\langle \sigma_s^2 \rangle \cong 1$ in (30), in which case this modified radiometric statistic is of little use.

Analysis and simulation results on the performances of the radiometer, modified radiometer, and single-cycle detectors (for various cycle frequencies) are presented in the following sections. The multicycle detector is excluded from the simulations because it is considerably more difficult to implement, since the absolute phase of the signal must be known (or estimated) for constructive addition of the terms in the sum over α in (17) [2], [4]. Before proceeding we explain the link between the single-cycle detector and two other methods of detection, which are based on the cyclic spectrum analyzer and the radar ambiguity function.

If the ideal spectral correlation function $S_s^\alpha(f)$ is unknown, we can replace it in the cycle detector (20) with a rectangular window with width on the order of the signal bandwidth, say, Δf. The resulting statistic is given by

$$y(t) = \frac{1}{\Delta f} \int_{f-\Delta f/2}^{f+\Delta f/2} S_{x_T}^\alpha(t,\nu)\, d\nu \triangleq S_{x_T}^\alpha(t,f)_{\Delta f}, \quad (33)$$

which is a standard frequency-smoothed estimate of the cyclic spectrum $S_x^\alpha(f)$ of the input waveform $x(t)$ [10]. The device that generates $y(t)$ in (33) for a range of values of f and α is called a *cyclic spectrum analyzer* (CSA), and is (with post-processing) capable of emulating all of the devices (17)–(20) as well as other quadratic detectors (16) [2]. The magnitude of the output of a CSA, for large time-frequency resolution product $T\Delta f$ (which ensures high-reliability measurements), and sufficiently small smoothing-window width Δf for adequate spectral resolution, when graphed as the height of a surface above the bifrequency plane, not only can provide a means for detection, but also, when compared to ideal SCF surfaces, can be used for signal recognition [14]. That is, the patterns of spectral correlation can be highly distinct for different modulation types even when the signals have identical power spectral densities. This is illustrated in [10] for BPSK, QPSK, SQPSK, MSK, FSK, AM, FM, PAM, PWM, PPM, and other modulation types. As an example, the ideal SCF surfaces for BPSK, QPSK, SQPSK, and MSK are shown in Fig. 1. Computationally efficient digital architectures for cyclic spectral analysis are developed in [15] (cf. [16]).

The spectral-correlation-function estimate (33) bears an interesting relationship to the function

$$R_{x_T}^\alpha(t,\tau) \triangleq \frac{1}{T} \int_{t-(T-|\tau|)/2}^{t+(T-|\tau|)/2} x(u+\tau/2) \cdot x^*(u-\tau/2) e^{-i2\pi\alpha u}\, du. \quad (34)$$

Specifically,

$$y(t) = \int_{-\infty}^{\infty} R_{x_T}^\alpha(t,\tau) \frac{\sin(\pi\Delta f\tau)}{\pi\tau} e^{-i2\pi f\tau}\, d\tau, \quad (35)$$

which is the Fourier transform of a windowed version of (34). Since (34) is the complex-valued radar ambiguity function for a sliding segment of data (when $x(t)$ is the analytic signal for the received waveform) where α is the range-rate (Doppler) parameter and τ is the range (delay) parameter, we see that the complex-valued spectral correlation surface is the Fourier transform of the windowed complex-valued ambiguity surface, which has been proposed for signal interception (e.g., [17]).

IV. Deflection

Because of its analytical tractability (relative to the probabilities required to construct the receiver operating characteristic), deflection is a commonly used performance indicator in the literature on signal interception [5]–[8]. In order to put this particular performance indicator into better perspective, its maximum possible value for signals in WGN is presented in this section. Then in Section V the relative deflection performances of several detectors are compared to their relative receiver operating characteristic (ROC) performances. Before proceeding, it is important to note that the detection statistic (20) of the cycle detector is complex-valued, and that the correct statistic to be used in the threshold test

$$y'_{sc} \underset{H_0}{\overset{H_1}{\gtrless}} \gamma \tag{36}$$

is the magnitude of the statistic (20),

$$y'_{sc} \triangleq |y_{sc}|. \tag{37}$$

To ensure mathematical tractability of the deflection, it is necessary to use y_{sc} in (21). This renders the resulting deflection formulas less useful than desired since they are based on a statistic that differs from the true detection statistic by the nonlinear operation $|\cdot|$. The justification for using y_{sc} is threefold. First, it can be shown that the deflection based on the real statistic y'_{sc}, denoted by d_r, is always larger than the deflection based on the complex statistic, denoted by d_c, provided that the length of the collect time T is sufficiently large (a proof of this is given in the Appendix). Thus, d_c is a reliably conservative measure of the performance of the cycle detector. Second, the evaluation of d_c provides a convenient and necessary means for checking the results of computer simulations, which are required to compute d_r and the probabilities of detection and false alarm, P_D and P_{FA}, for ROC's. Third, the study of deflection provides a unifying link with previous SNR studies of weak-signal detection [5]–[8].

A. Constant WGN Background

It is shown in [2] that the deflection d for the weak-signal likelihood-ratio detector (which maximizes deflection) for a WGN background is given by

$$\begin{aligned} d^2_{\max} &= \frac{1}{2N_0^2} \int_{-T/2}^{T/2} \int_{-T/2}^{T/2} [R_s(t-u, t-v)]^2 \, du \, dv \\ &= \frac{1}{2N_0^2} \sum_{\alpha,\beta} \int_{-T}^{T} R_s^{\alpha}(\tau) R_s^{\beta}(\tau) \\ &\quad \cdot \frac{\sin[\pi(\alpha+\beta)(T-|\tau|)]}{\pi(\alpha+\beta)} \, d\tau e^{-i2\pi(\alpha+\beta)t} \\ &\cong \frac{T}{2N_0^2} \sum_{\alpha} \int_{-T}^{T} |R_s^{\alpha}(\tau)|^2 \, d\tau \\ &\cong \frac{T}{2N_0^2} \sum_{\alpha} \int_{-\infty}^{\infty} |S_s^{\alpha}(f)|^2 \, df. \end{aligned} \tag{38}$$

This approximation is accurate if T is sufficiently large relative to the longest period of cyclostationarity ($T \gg 1/\alpha_{\min}$), and sufficiently large relative to the largest width of the cyclic autocorrelations $R_s^{\alpha}(\tau)$. It is also shown in [2] that the deflection $d(\alpha)$ of the single-cycle detector (which equals the maximized SNR of the spectral line regenerator referred to in Section III) is given by

$$d^2(\alpha) = \frac{T}{2N_0^2} \int_{-\infty}^{\infty} |S_s^{\alpha}(f)|^2 \, df. \tag{39}$$

Consequently,

$$d^2_{\max} \cong \sum_{\alpha} d^2(\alpha). \tag{40}$$

These deflection formulas are evaluated in [18] for BPSK, QPSK, SQPSK (each with rectangular pulse shape), and MSK (SQPSK with a half-cycle cosine pulse shape) and the results are summarized here in Table I.

B. Variable WGN Background

Let us now consider the problem of detecting a cyclostationary signal in broad-band noise with variable level. The noise is modeled as white and Gaussian with the spectral height N_0 modeled as the square of a Gaussian variate with parameters $\mu_N \triangleq E\{N_0\}$, $\sigma_N^2 \triangleq E\{N_0^2\} - \mu_N^2$, and $\rho_N \triangleq \sigma_N^2/\mu_N^2$ where ρ_N is the coefficient of variation of N_0. It is shown in [19] that the deflections are given by

$$\tilde{d}(0) \cong \frac{\mathrm{SNR_{in}} d_0(0) \sqrt{\frac{T}{T_c}}}{\left[1 + \rho_N \left(1 + \frac{3T}{2T_c}\right)\right]^{1/2}} \tag{41}$$

for the radiometer and

$$\tilde{d}(\alpha) \cong \frac{\mathrm{SNR_{in}} d_0(\alpha) \sqrt{\frac{T}{T_c}}}{(1+\rho_N)^{1/2}} \tag{42}$$

for the cycle detector where

$$\mathrm{SNR_{in}} \triangleq \frac{P_s}{\left(\frac{2}{T_c}\right)\mu_N} \tag{43}$$

$$d_0(\alpha) = \begin{cases} 1/\pi, & \alpha = 1/T_c \\ 1/\sqrt{3}, & \alpha = 2f_0 \\ \sqrt{2}/\sqrt{3} & \alpha = 0, \end{cases} \tag{44}$$

and P_s is the average signal power. The value of the coefficient $d_0(\alpha)$ for any particular α is proportional to the strength of the cyclic feature associated with that α,

$$d_0(\alpha) \propto \left[\int_{-\infty}^{\infty} |S_s^{\alpha}(f)|^2 \, df \right]^{1/2}, \tag{45}$$

and is equal to the deflection $d(\alpha)$, normalized by $\mathrm{SNR_{in}} \cdot \sqrt{T/T_c}$, for the cycle detector when N_0 is nonrandom

TABLE I
NORMALIZED DEFLECTION $d_0(\alpha)$ FOR THE RADIOMETER ($\alpha = 0$) AND SINGLE-CYCLE DETECTORS ($\alpha \neq 0$) FOR NO NOISE VARIABILITY, $\rho_N = 0$. THESE EXACT RESULTS ARE NOT IN COMPLETE AGREEMENT WITH APPROXIMATE RESULTS OBTAINED ELSEWHERE AND REPRODUCED IN [23, TABLE 4.3]. THESE RESULTS ALSO DIFFER SUBSTANTIALLY IN SOME CASES (E.G., SQPSK) FROM RESULTS OBTAINED ELSEWHERE FOR SUBOPTIMUM AD HOC DETECTORS, AS REPRODUCED IN [23, TABLE 4.3]

α	Normalized Deflection BPSK	QPSK	SQPSK	MSK
Multi-Cycle	$\sqrt{2}$ (3 dB)	1 (0 dB)	1 (0 dB)	1 (0 dB)
0	$\sqrt{2/3}$ (−1.76 dB)	$\sqrt{2/3}$ (−1.76 dB)	$\sqrt{2/3}$ (−1.76 dB)	$\frac{1}{2}\left[\frac{4}{3} + \frac{10}{\pi^2}\right]^{1/2}$ (−2.32 dB)
$1/T_c$	$1/\pi$ (−9.90 dB)	$1/\pi$ (−9.90 dB)	0	0
$2/T_c$	$1/2\pi$ (−16.0 dB)	$1/2\pi$ (−16.0 dB)	$1/2\pi$ (−16.0 dB)	$\frac{1}{2\pi}\sqrt{5/18}$ (−21.5 dB)
$2f_0$	$1/\sqrt{3}$ (−4.77 dB)	0	0	0
$2f_0 + 1/T_c$	$1/\pi\sqrt{2}$ (−12.9 dB)	0	$1/\pi\sqrt{2}$ (−12.9 dB)	$\frac{1}{2}\left[\frac{1}{3} + \frac{5}{8\pi^2}\right]^{1/2}$ (−10.0 dB)

($\rho_N = 0$). The formulas (41) and (42) are accurate if the collect time T satisfies the following conditions:

$$T \gg \max_{\alpha} \{\tau_\alpha\} \tag{46a}$$

$$T \gg \frac{1}{\alpha + \beta} \tag{46b}$$

where β represents all cycle frequencies ($\beta \neq -\alpha$) associated with the SOI $s(t)$ and τ_α is the width of the cyclic autocorrelation $R_s^\alpha(\tau)$. In addition, it is required that $f_0 T_c \gg 1$.

Approximations (41) and (42) indicate that the radiometer yields the largest deflection for $\rho_N = 0$, but that both the doubled-carrier cycle detector ($\alpha = 2f_0$) and the chip-rate cycle detector ($\alpha = 1/T_c$) can have much larger deflection than that of the radiometer for $\rho_N \neq 0$ and large T. These considerations lead to the conclusion that the cycle detectors can have superior performance relative to the radiometer when the collect time is long (as it needs to be for weak-signal detection). This prediction is confirmed by the receiver operating characteristics presented in the next section.

V. RECEIVER OPERATING CHARACTERISTICS

In this section, the results of computer simulations of the four detectors under study—the radiometer, modified radiometer, and cycle detectors for the chip rate and doubled carrier frequency—are presented. The detectors simulated are (30) and the discrete-time counterparts of the continuous-time detectors (19) and (20). These counterparts are obtained by replacing the integrals by sums and implementing the Fourier transform (7), which occurs in the cyclic periodogram, with an FFT algorithm.

In order to obtain the probabilities of detection P_D and false alarm P_{FA} needed to form the ROC, it is necessary to generate many sample paths of the signal and noise processes in order to obtain adequate sample sets of the detection statistics. The generated statistics are compared to thresholds to estimate the required probabilities. For the results presented here, 1000 sample paths for each hypothesis were used. Both BPSK and QPSK SOIs are considered. For the case of $\rho_N = 0$, the value of the noise spectal height is fixed from trial to trial, whereas when $\rho_N \neq 0$, the value of N_0 is chosen randomly at the beginning of each trial and is fixed for that trial. The random variable N_0 is the square of a Gaussian variate, with mean and coefficient of variation given by

$$\mu_N = E\{N_0\},$$

and

$$\rho_N = \frac{E\{N_0^2\} - \mu_N^2}{\mu_N^2}.$$

Thus, when $\rho_N = 0$, N_0 is nonrandom and has value μ_N.

The first cases of interest include both long and short collection times combined with zero-to-moderate noise-level variability for an SNR of 0 dB [cf. (43)]. Fig. 2 shows the ROC's, which plot P_D against P_{FA}, for long collect, $T =$ 128 chips, and moderate variability, $\rho_N = 0.1$. In this and all figures, the radiometer is represented by a thick solid line, the chip-rate ($\alpha = 1/T_c$) cycle detector by a medium-thickness line, the doubled-carrier ($\alpha = 2f_0$) cycle detector by a line with small circles, and the modified radiometer by a thin line. In Fig. 2, the modified radiometer and the doubled-carrier cycle detector have ROC's that are nearly indistinguishable (uppermost curve). The performances of these two detectors are almost identical and are far superior to both the chip-rate cycle detector and the radiometer. The chip-rate cycle detector, however, is greatly superior to the radiometer. For example, for a false alarm probability of $P_{FA} = 0.025$, the radiometer has a probability of detection of $P_D = 0.39$, whereas the chip-rate cycle detector has $P_D = 0.94$. It is evident that

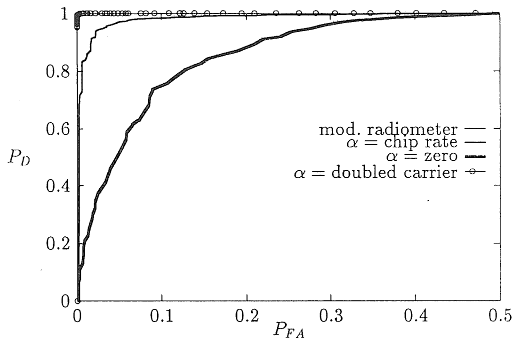

Fig. 2. Receiver operating characteristics for BPSK SOI. SNR = 0 dB, $\rho_N = 0.1$, $T = 128\ T_c$.

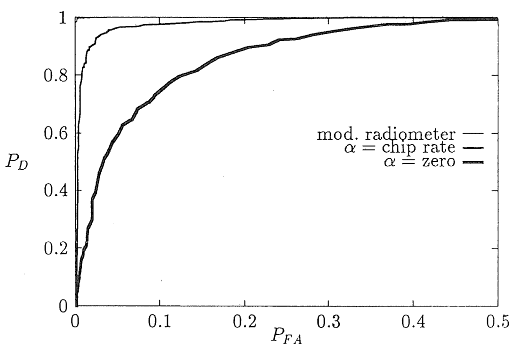

Fig. 3. Receiver operating characteristics for QPSK SOI. SNR = 0 dB, $\rho_N = 0.1$, $T = 128\ T_c$.

the performance predictions from the previous section based on deflection are substantiated for long collect and non-zero variability. This case was repeated using a QPSK SOI. The resulting ROC's are shown in Fig. 3. The performance of the detectors for this SOI is nearly identical to that for the BPSK SOI (Fig. 2) because the two signals have the same SCF for $\alpha = k/T_c$. The ROC for the doubled-carrier feature detector is absent for the QPSK signal because there is no cyclic feature at $\alpha = 2f_0$.

To further illustrate the superiority of the cycle detector over the radiometer, histograms of the generated detection statistics are presented. The histograms plot the frequency of occurrence of values within amplitude bins for each statistic versus the bin location. For the case corresponding to the ROCs in Fig. 2, the histograms in Figs. 4 and 5 for $\alpha = 2f_0$ and $\alpha = 0$, respectively, are obtained. The separation between the peaks in Fig. 4 is quite clear, whereas there is no discernible separation of peaks for the radiometer, Fig. 5.

In the next case, summarized in Fig. 6, the collect is reduced to 16 chips, while all other parameters are kept the same. The modified radiometer is clearly superior, followed in descending order by the doubled-carrier cycle detector, radiometer, and chip-rate cycle detector. Although the modified radiometer outperforms both cycle detectors in this case, the ROC's in Fig. 7 shows that the order of performance of the detectors reverses for increased fractional bandwidth (increased from 1/4 to 2/3), as explained in Section III.

An interesting and revealing case involves very short collect, $T = 4$ chips, and zero variability, $\rho_N = 0$, with

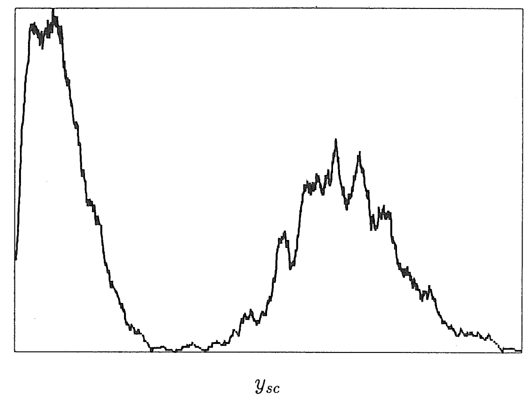

Fig. 4. Histogram of detection statistics for BPSK SOI with $\alpha = 2f_0$, SNR = 0 dB, $\rho_N = 0.1$, $T = 128\ T_c$.

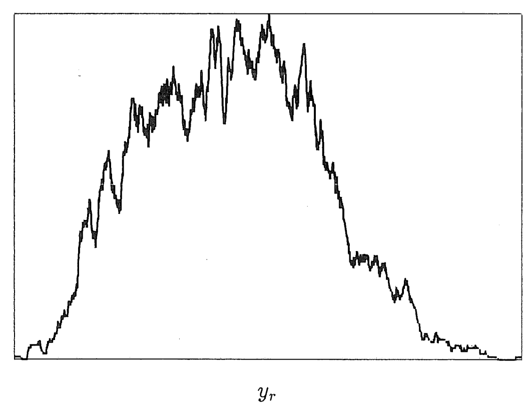

Fig. 5. Histogram of detection statistics for BPSK SOI with $\alpha = 0$, SNR = 0 dB, $\rho_N = 0.1$, $T = 128\ T_c$.

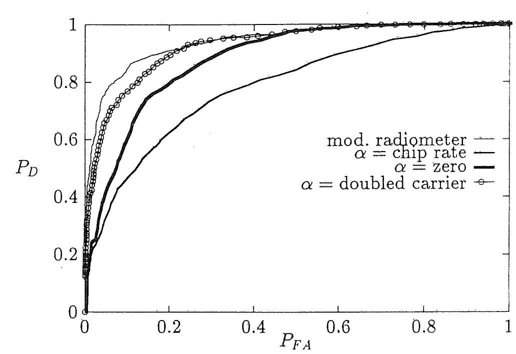

Fig. 6. Receiver operating characteristics for BPSK SOI. SNR = 0 dB, $\rho_N = 0.1$, $T = 16\ T_c$, fractional bandwidth = 1/4.

SNR = 5 dB. This corresponds to the type of situation in which the radiometer is expected to outperform all other detectors (based on the analysis of the deflection in Section IV). However, as evidenced by the ROC's in Fig. 8, the doubled-carrier cycle detector is seen to be slightly superior to the optimum radiometer. The fact that the cycle detector can be competitive with the radiometer in calm environments with short collect time points out the drawbacks of the deflection as a performance indicator (at least when applied to a complex detection statistic).

Finally, the case of narrowband (sinusoidal) interferers spread across the entire receiver band that are randomly

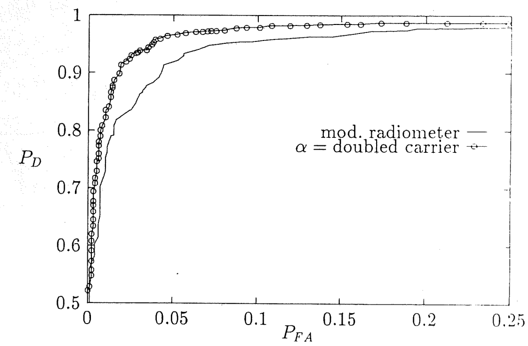

Fig. 7. Receiver operating characteristics for BPSK SOI. SNR = 0 dB, $\rho_N = 0.1$, $T = 43\ T_c$, fractional bandwidth = 2/3.

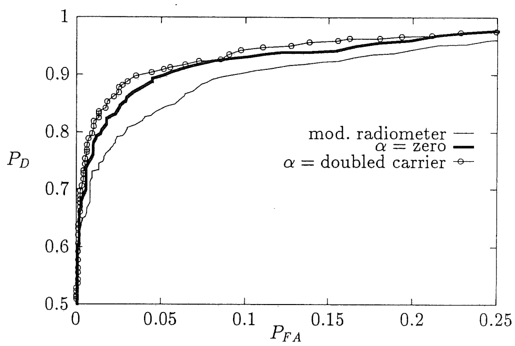

Fig. 8. Receiver operating characteristics for BPSK SOI. SNR = 5 dB, $\rho_N = 0$, $T = 4\ T_c$.

switched off and on (so that only one interferer is present at any given time) is considered. The switching rate is small compared to the carrier frequency f_0 and the chip rate $1/T_c$ so that the measured power spectra of the interferer for a set of collects with lengths of interest is a set of relatively narrow-width spikes distributed across the receiver band. ROC's for the case of very small signal-to-interference ratio, SIR = −10 dB, and moderate collect, $T = 64$ chips, and SNR = 10 dB are given in Fig. 9. The performance advantage of the chip-rate detector is extreme in this case. (Since the performance of the doubled-carrier detector is so much better than both the radiometer and chip-rate detector, its ROC, which is nearly equal to unity for all P_{FA}, is not shown.) For small collect, $T = 16$ chips, SIR = 0 dB, and SNR = 10 dB, the ROC's in Fig. 10 for a BPSK SOI and Fig. 11 for a QPSK SOI are obtained. For small probabilities of false alarm, say $P_{FA} < 0.12$, both cycle detectors outperform the radiometer for both modulation types.

VI. Conclusion

It is shown in this paper by simulation and analysis that cycle detectors can outperform the radiometer and the joint signal detection and noise-level estimation radiometric detector (modified radiometer) when the background noise or interference is variable. It is also shown by simulation that the cycle detector can in some cases outperform the optimum radiometer even when the variability of the background noise is zero. This latter result is based not on measured deflection, but rather on the measured error probabilities as reflected in the

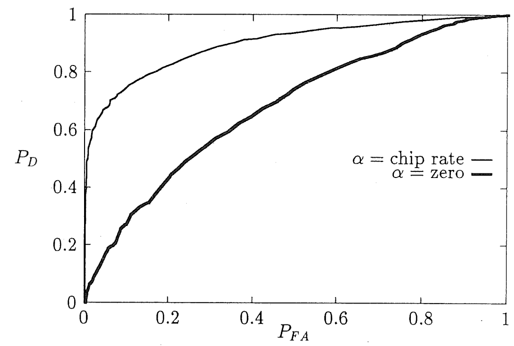

Fig. 9. Receiver operating characteristics for BPSK SOI. SNR = 10 dB, SIR = −10 dB, $\rho_N = 0$, $T = 64\ T_c$, random-location narrow-band interferer.

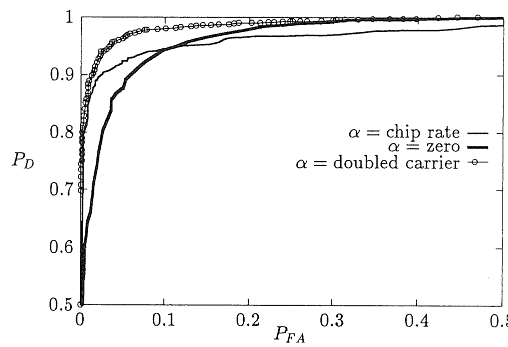

Fig. 10. Receiver operating characteristic for BPSK SOI. SNR = 10 dB, SIR = 0 dB, $\rho_N = 0$, $T = 16\ T_c$, random-location narrow-band interferer.

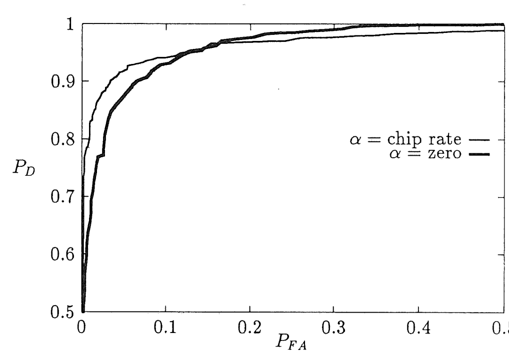

Fig. 11. Receiver operating characteristics for QPSK SOI. SNR = 10 dB, SIR = 0 dB, $\rho_N = 0$, $T = 16\ T_c$, random-location narrow-band interferer.

receiver operating characteristic. This result is not predicted by theoretical calculations of the deflection. Thus, whereas the deflection is useful in deriving detectors (which can be derived other ways as well), it is not always appropriate for performance comparisons with other detectors (cf. [5]).

In conclusion, cyclic spectral analysis in general and the cycle detectors in particular possess substantial performance advantages over more conventional signal processing methods for interception of direct-sequence spread-spectrum signals. However, the cycle detection methods do require that the signal of interest exhibit cyclostationarity, and the single-cycle detectors also require knowledge of the value of a cycle frequency. Thus, modifications of the modulation schemes, which produce the spread-spectrum signals, that destroy, substantially weaken, or vary the cyclostationarity of the signal are needed to prevent interception by cycle detection. Such modifications are the subject of current research by the authors [21], [22].

APPENDIX
PROOF THAT $d_c \leq d_r$

In this Appendix, it is proved that the deflection based on the complex detection statistic d_c is less than the deflection based on the magnitude of that statistic d_r, as asserted in Section IV. The required condition is that the collect time T of the detector be sufficiently large.

In this proof, the averages in the definition of deflection are taken to be averages over a finite set of complex numbers (random samples), rather than over an abstract probability space with a probability weighting function. This is the way the deflection is computed from simulations or from data, rather than the way it is analytically calculated using expectations. Also, the fact that the magnitude of the average of n complex numbers is less than or equal to the average of the magnitudes of the numbers is used:

$$\left|\frac{1}{n}\sum_{i=1}^{n} z_i\right| \leq \frac{1}{n}\sum_{i=1}^{n}|z_i|. \tag{A1}$$

Proof: The numerator of the complex deflection is given by

$$\mathrm{num}_c = \frac{1}{n}\left|\sum_{i=1}^{n}(y_i|H_1) - \sum_{i=1}^{n}(y_i|H_0)\right|. \tag{A2}$$

Using (A1), we obtain

$$\begin{aligned}\mathrm{num}_c &\leq \frac{1}{n}\left|\sum_{i=1}^{n}(y_i|H_1)\right| + \frac{1}{n}\left|\sum_{i=1}^{n}(y_i|H_0)\right| \\ &\leq \frac{1}{n}\sum_{i=1}^{n}\left(|y_i| \mid H_1\right) + \frac{1}{n}\sum_{i=1}^{n}\left(|y_i| \mid H_0\right).\end{aligned} \tag{A3}$$

If the condition

$$\sum_{i=1}^{n}\left(|y_i| \mid H_0\right) \ll \sum_{i=1}^{n}\left(|y_i| \mid H_1\right) \tag{A4}$$

is met, then we can make the close approximation

$$\begin{aligned}\frac{1}{n}\sum_{i=1}^{n}\left(|y_i| \mid H_1\right) + \frac{1}{n}\sum_{i=1}^{n}\left(|y_i| \mid H_0\right) \cong \frac{1}{n}\sum_{i=1}^{n}\left(|y_i| \mid H_1\right) \\ -\frac{1}{n}\sum_{i=1}^{n}\left(|y_i| \mid H_0\right) = \mathrm{num}_r.\end{aligned} \tag{A5}$$

where num_r is the numerator of the real deflection. The condition (A4) will be met for sufficiently long collection time because the noise does not exhibit cyclostationarity, and thus the detection statistic on the null hypothesis actually vanishes when the collection time increases without bound. Thus, we have the approximate inequality $\mathrm{num}_r \gtrsim \mathrm{num}_c$, which becomes a strict inequality asymptotically. Furthermore, we have

$$\mathrm{den}_c = \mathrm{Var}(y|H_0) = \frac{1}{n}\sum_{i=1}^{n}\left(|y_i|^2|H_0\right) - \left|\frac{1}{n}\sum_{i=1}^{n}(y_i|H_0)\right|^2 \tag{A6}$$

and

$$\begin{aligned}\mathrm{den}_r = \mathrm{Var}\left(|y| \mid H_0\right) = \frac{1}{n}\sum_{i=1}^{n}\left(|y_i|^2|H_0\right) \\ -\left[\frac{1}{n}\sum_{i=1}^{n}\left(|y_i| \mid H_0\right)\right]^2.\end{aligned} \tag{A7}$$

Using (A1), we obtain

$$\frac{1}{n}\sum_{i=1}^{n}\left(|y_i| \mid H_0\right) \geq \left|\frac{1}{n}\sum_{i=1}^{n}(y_i|H_0)\right| \tag{A8}$$

and therefore the variance of the real statistic $|y_i|$ is always *smaller* than that for the complex statistic y_i, thus $\mathrm{den}_r \leq \mathrm{den}_c$. Since the numerator of the real deflection is larger for sufficiently long collect time, and the denominator is smaller, it follows that $d_c \leq d_r$ for sufficiently long collection time.

ACKNOWLEDGMENT

The authors gratefully acknowledge C. K. Chen and L. Paura for their assistance in calculating deflection [18], [20].

REFERENCES

[1] W. A. Gardner, "Stationarizable random processes," *IEEE Trans. Inform. Theory,* vol. IT-24, pp. 8–22, 1978.
[2] ——, "Signal interception: A unifying theoretical framework for feature detection," *IEEE Trans. Commun.,* vol. 36, pp. 897–906, Aug. 1988.
[3] W. A. Gardner and C. K. Chen, "Signal-selective time-difference-of-arrival estimation for passive location of manmade signal sources in highly corruptive environments. Part I: Theory and method; Part II: Algorithms and performance," *IEEE Trans. Signal Processing,* vol. 40, 1992.
[4] W. A. Gardner, *Introduction to Random Processes with Applications to Signals and Systems.* New York: McGraw-Hill, 1989, 2nd ed.
[5] ——, "A unifying view of second-order measures of quality for signal classification," *IEEE Trans. Commun.,* vol. COM-28, pp. 807–816, June 1980.
[6] N. F. Krasner, "Optimal detection of digitally modulated signals," *IEEE Trans. Commun.,* vol. COM-30, pp. 885–895, May 1982.
[7] A. Polydoros and C. L. Weber, "Detection performance considerations for direct-sequence and time-hopping LPI waveforms," *IEEE J. Select. Areas Commun.,* vol. SAC-3, pp. 727–744, Sept. 1985.
[8] B. Picinbono and P. Duvaut, "Optimal linear-quadratic systems for detection and estimation," *IEEE Trans. Inform. Theory,* vol. 34, pp. 304–311, Mar. 1988.
[9] W. A. Gardner, "Exploitation of spectral redundancy in cyclostationary signals," *IEEE Signal Processing Mag.,* vol. 8, pp. 14–36, Apr. 1991.
[10] ——, *Statistical Spectral Analysis: A Nonprobabilistic Theory.* Englewood Cliffs, NJ: Prentice-Hall, 1987.
[11] H. L. Van Trees, *Detection, Estimation, and Modulation Theory, Part III.* New York: Wiley, 1971.
[12] W. A. Gardner, "Structural characterization of locally optimum detectors in terms of locally optimum estimators and correlators," *IEEE Trans. Inform. Theory,* vol. IT-28, pp. 924–932, Nov. 1982.
[13] D. Middleton, "Canonically optimum threshold detection," *IEEE Trans. Inform. Theory,* vol. IT-12, pp. 230–243, Apr. 1966.
[14] W. A. Gardner, "Measurement of spectral correlation," *IEEE Trans. Acoust., Speech, Signal Processing,* vol. ASSP-34, pp. 1111–1123, Oct. 1986.
[15] R. S. Roberts, "Digital architectures for cyclic spectral analysis," Ph.D. dissertation, Dep. Elec. Eng. Comput. Sci., Univ. California, Davis, Sept. 1989.
[16] R. S. Roberts, W. A. Brown, and H. H. Loomis, Jr., "Computationally efficient algorithms for cyclic spectral analysis" *IEEE Signal Processing Mag.,* vol. 8, pp. 38–49, Apr. 1991.
[17] S. Stein, "Algorithms for ambiguity function processing," *IEEE Trans. Acoust., Speech, Signal Processing,* vol. ASSP-29, pp. 588–599, June 1981.

[18] C. K. Chen, "Spectral correlation characterization of modulated signals with application to signal detection and source location," Ph.D. dissertation, Dep. Elec. Eng. Comput. Sci., Univ. California, Davis, Mar. 1989.
[19] C. M. Spooner, "Performance evaluation of detectors for cyclostationary signals," M.S. thesis, Dep. Elec. Eng. Comput. Sci., Univ. California, Davis, June 1988.
[20] W. A. Gardner and L. Paura, "Signal interception: Performance advantages of cycle detectors," in *Proc. Onzième Colloque sur le Traitement du Signals et des Images (GRETSI),* Nice, France, June 1–5, 1987, pp. 135–138.
[21] W. A. Gardner and C. M. Spooner, "Higher order cyclostationarity, cyclic cumulants and cyclic polyspectra," in *Proc. Int. Symp. Inform. Theory Appl.,* Hawaii, Nov. 27–30, 1990, pp. 355–358.
[22] C. M. Spooner and W. A. Gardner, "An overview of the theory of higher-order cyclostationarity," in *Proc. NASA/Hampton University, Workshop on Nonstationary Random Processes,* Hampton, VA, Aug. 1–2, 1991.
[23] D. L. Nicholson, *Spread Spectrum Signal Design, LPE and AJ Systems.* Rockville, MD: Computer Science, 1988.

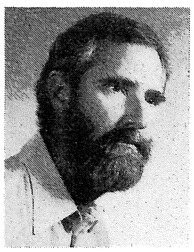

William A. Gardner (S'64–M'67–SM'84–F'91) was born in Palo Alto, CA, on November 4, 1942. He received the M.S. degree from Stanford University, in 1967, and the Ph.D. degree from the University of Massachusetts, Amherst, in 1972, both in electrical engineering.

He was a Member of the Technical Staff at Bell Laboratories in Massachusetts from 1967 to 1969. He has been a faculty member at the University of California, Davis, since 1972, where he is Professor of Electrical Engineering and Computer Science. Since 1982, he has also been President of the engineering consulting firm Statistical Signal Processing, Inc., Yountville, CA. His research interests are in the general area of statistical signal processing, with primary emphasis on the theories of time-series analysis, stochastic processes, and signal detection and estimation.

Dr. Gardner is the author of *Introduction to Random Processes with Applications to Signals and Systems* (Macmillan, 1985, second edition, McGraw-Hill, 1990), *The Random Processes Tutor: A Comprehensive Solutions Manual for Independent Study* (McGraw-Hill, 1990), and *Statistical Spectral Analysis: A Nonprobabilistic Theory,* (Prentice-Hall, 1987). He holds several patents and is the author of numerous research-journal papers. He received the Best Paper of the Year Award from the European Association for Signal Processing in 1986 for the paper entitled "The Spectral Correlation Theory of Cyclostationary Signals," the 1987 Distinguished Engineering Alumnus Award form the University of Massachusetts, and the Stephen O. Rice Prize Paper Award in the Field of Communication Theory from the IEEE Communications Society in 1988 for the paper entitled "Signal interception: A unifying theoretical framework for feature detection," He is a member of the American Mathematical Society, the Mathematical Association of America, the American Association for the Advancement of Science, and the European Association for Signal Processing, and is a member of the honor societies Sigma Xi, Tau Beta Pi, Eta Kappa Nu, and Alpha Gamma Sigma.

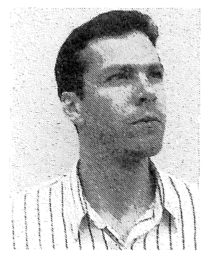

Chad M. Spooner (S'91) was born in Des Moines, IA, on October 5, 1963. He received the A.S. degree with high honors from Santa Rosa Junior College in 1984. He received the B.S. degree from the University of California at Berkeley in 1986, and the M.S. degree from University of California at Davis in 1988, both in electrical engineering. Since 1988 he has been engaged in doctoral research at UC Davis in electrical engineering.

He was a Teaching Assistant in the Department of Electrical Engineering and Computer Science from 1986 to 1988. Since 1988 he has been a Research Assistant at UC Davis, and a consultant to Statistical Signal Processing, Inc. He is coauthor of a unique, commercially available, cyclic spectral analysis software package. His research interests include statistical signal processing, weak-signal detection and parameter estimation, and the theory of higher order cyclostationarity.